BIT Numerical Mathematics (2024) 64:7
https://doi.org/10.1007/s10543-024-01008-x

BIT

A posteriori error estimates for a dual finite element method for singularly perturbed reaction–diffusion problems

JaEun Ku[1] · **Martin Stynes**[2]

Received: 29 August 2023 / Accepted: 8 January 2024 / Published online: 5 February 2024
© The Author(s), under exclusive licence to Springer Nature B.V. 2024

Abstract
A posteriori error estimates are established for a two-step dual finite element method for singularly perturbed reaction–diffusion problems. The method can be considered as a modified least-squares finite element method. The least-squares functional is the basis for our residual-type a posteriori error estimators, which are shown to be reliable and efficient with respect to the error in an energy-type norm. Moreover, guaranteed upper bounds for the errors in the computed primary and dual variables are derived; these bounds are then used to drive an adaptive algorithm for our finite element method, yielding any desired accuracy. Our theory does not require the meshes generated to be shape-regular. Numerical experiments show the effectiveness of our a posteriori estimators.

Keywords Singularly perturbed · Reaction–diffusion · A posteriori estimates · Dual finite element method

Mathematics Subject Classification 65N30 · 65N15

Communicated by Rolf Stenberg.

JaEun Ku's research is supported by NSF Grant DMS-2208289. The work of Martin Stynes is supported in part by the National Natural Science Foundation of China under Grants 12171025 and NSAF-U2230402.

✉ Martin Stynes
m.stynes@csrc.ac.cn

JaEun Ku
jku@okstate.edu

[1] Department of Mathematics, Oklahoma State University, 401 Mathematical Sciences, Stillwater, OK 74078, USA

[2] Applied and Computational Mathematics Division, Beijing Computational Science Research Center, Beijing 100193, China

1 Introduction

Consider the singularly perturbed reaction–diffusion problem

$$-\varepsilon^2 \triangle u + \frac{1}{b}\, u = f \ \text{ in } \Omega, \qquad u = 0 \ \text{ on } \partial\Omega, \tag{1.1}$$

where $0 < \varepsilon \ll 1$, $b \in L_\infty(\Omega)$ satisfies $0 < b_{\min} \le b \le b_{\max} < \infty$, and $\Omega \subset \mathbb{R}^n$ for $n = 2, 3$ is a bounded polygonal domain or a smooth domain, with boundary $\partial\Omega$. Here ε, $b_{\min}$ and $b_{\max}$ are constants that are independent of $x \in \Omega$. Furthermore, the ratio $b_{\max}/b_{\min}$ is independent of ε; for simplicity we assume that $b_{\max}/b_{\min} = \mathcal{O}(1)$. Typical solutions of (1.1) exhibit boundary and/or interior layers and other forms of local behavior.

See [20] and its references for an overview of numerical methods for singularly perturbed problems. It is clearly desirable to have adaptive procedures to compute approximate solutions of such problems.

Much work has gone into the development of reliable and efficient a posteriori error estimators for finite element methods (FEMs) used to solve singularly perturbed problems. For energy-type norms, Verfürth [24] was the first to derive reliable and efficient a posteriori error estimators, using bubble functions. Ainsworth and Babuška [1] presented error estimators based on equilibrated residuals, under the assumption that a local boundary value problem is solved exactly over each element, which limits the practical application of the method. This work was extended by Ainsworth and Vejchodský [2, 3] to fully computable, reliable upper bounds that do not require exact solution of a local problem. Smears and Vohralík [22] use a $H(\mathrm{div})$ conforming flux reconstruction to derive a posteriori error estimators that do not require any local submesh yet produce reliable and efficient equilibrated flux estimators for arbitrary-order approximations; this work is based on an idea of Cheddadi et al. [6]. For maximum norm error estimates, Demlow and Kopteva [10, 15] obtained a posteriori error estimators using bounds for the Green's function of (1.1) on shape-regular locally uniform meshes, but in [16] are extended to piecewise linear FEMs on anisotropic meshes. See also [9, 17, 24, 26] and their references.

All these papers deal with conforming FEMs; for nonconforming FEMs see [26] and the literature review in its Introduction.

The estimators in the papers above are based on Galerkin FEMs. In contrast, the estimators that we shall present here are based on a dual FEM for singularly perturbed reaction–diffusion problems that was analysed recently in [5]. As shown in [5], the solution of this dual FEM does not display significant numerical oscillations, unlike the standard Galerkin methods. The method computes an approximation of the dual variable $\boldsymbol{\sigma} := -\nabla u$, then the primary variable u is recovered in an efficient manner. The algebraic system associated with the dual variable is symmetric and positive definite, and there are well-developed solvers for such systems. This dual FEM is a competitive alternative to standard and mixed Galerkin FEMs for problems such as (1.1), but it should be mentioned that the dual FEM has a larger number of degrees of freedom than the standard Galerkin method.

Our goal in the present paper is to develop reliable and efficient residual-type a posteriori error estimators for the dual FEM applied to (1.1) on geometrically conformal meshes [14, Section 1.3.3] (for such meshes, roughly speaking, hanging nodes are forbidden but the mesh is not required to be shape-regular, i.e., it can be anisotropic). The dual FEM can be regarded as a modified least-squares method, and a notable advantage of least-squares methods is that the least-squares functional can be used as a built-in residual-type a posteriori error estimator. We shall exploit this property.

Standard notation for Sobolev spaces will be used, e.g., $H(\mathrm{div}) = \{\boldsymbol{\tau} \in L_2^d(\Omega) : \nabla \cdot \boldsymbol{\tau} \in L_2(\Omega)\}$. For $i \geq 0$, let $\|\cdot\|_i$ denote the $W_2^i(\Omega)$ norm. Thus, $\|\cdot\|_0$ denotes the $L_2(\Omega)$ norm.

Define the norm $|||(\cdot,\cdot)|||$ by

$$|||(\boldsymbol{\tau}, v)|||^2 = \|\varepsilon\, b\, \nabla\cdot\boldsymbol{\tau}\|_0^2 + \|\boldsymbol{\tau}\|_0^2 + \|\varepsilon\nabla v\|_0^2 + \|v\|_0^2 \quad \forall (\boldsymbol{\tau}, v) \in H(\mathrm{div}) \times H_0^1(\Omega). \tag{1.2}$$

This norm is an extension of the standard energy-type norm $v \mapsto \left(\|\varepsilon\nabla v\|_0^2 + \|v\|_0^2\right)^{1/2}$.

Define a functional $\eta \geq 0$ on $H(\mathrm{div}) \times H_0^1(\Omega)$ by

$$\eta^2(\boldsymbol{\tau}, v) = \|\varepsilon\, b\, \nabla\cdot\boldsymbol{\tau} + v\|_0^2 + \|\boldsymbol{\tau} + \varepsilon\nabla v\|_0^2 \quad \forall (\boldsymbol{\tau}, v) \in H(\mathrm{div}) \times H_0^1(\Omega). \tag{1.3}$$

We shall say that a quantity is *guaranteed* if it can be evaluated using the computed numerical solution and does not contain any unknown constants.

The dual FEM computes a solution $(\boldsymbol{\sigma}_h, u_h) \in H(\mathrm{div}) \times L_2(\Omega)$ that approximates $(\boldsymbol{\sigma}, u)$. One cannot apply the least-squares functional (1.3) and the norm $|||(\cdot,\cdot)|||$ to this computed solution because in general u_h lies only in $L_2(\Omega)$, not in $H_0^1(\Omega)$. A workaround is to instead use $\mathscr{I}^{CL}u_h \in H_0^1(\Omega)$, where $\mathscr{I}^{CL}$ denotes the Clément interpolation operator (see [14, Section 1.6.1] for its definition and properties). Thus (1.3) is used to define the following guaranteed residual-type error estimator:

$$\eta^2\left(\varepsilon(\boldsymbol{\sigma}-\boldsymbol{\sigma}_h), u - \mathscr{I}^{CL}u_h\right) = \left\| b\, f - \varepsilon^2\, b\nabla\cdot\boldsymbol{\sigma}_h - \mathscr{I}^{CL}u_h \right\|_0^2 + \varepsilon^2 \left\| \boldsymbol{\sigma}_h + \nabla\mathscr{I}^{CL}u_h \right\|_0^2, \tag{1.4}$$

where $\boldsymbol{\sigma} = -\nabla u$ and (1.1) were used to simplify the right-hand side. This fully-computable estimator is reliable and efficient, because Theorem 3.1 shows that

$$\frac{1}{2}\eta^2\left(\varepsilon(\boldsymbol{\sigma}-\boldsymbol{\sigma}_h), u - \mathscr{I}^{CL}u_h\right) \leq \left|\!\left|\!\left| \left(\varepsilon(\boldsymbol{\sigma}-\boldsymbol{\sigma}_h), u - \mathscr{I}^{CL}u_h\right) \right|\!\right|\!\right|^2 \leq \left(3\,\frac{\max\{1, b_{\max}\}}{\min\{1, b_{\min}\}} + 2\right)\eta^2\left(\varepsilon(\boldsymbol{\sigma}-\boldsymbol{\sigma}_h), u - \mathscr{I}^{CL}u_h\right).$$

Remark 1.1 In (1.4) note that the flux approximation error $\boldsymbol{\sigma} - \boldsymbol{\sigma}_h$ is scaled by ε. In Sect. 3, we will establish that for all $(\boldsymbol{\tau}, v)$ the functional $\eta^2(\boldsymbol{\tau}, v)$ [defined in (1.3)] is equivalent to the energy-type norm $|||(\boldsymbol{\tau}, v)|||^2$ that was defined in (1.2). Hence $\eta^2(\varepsilon(\boldsymbol{\sigma}-\boldsymbol{\sigma}_h), u - \mathscr{I}^{CL}u_h)$ is equivalent to $\|\varepsilon^2 b\,\nabla\cdot(\boldsymbol{\sigma}-\boldsymbol{\sigma}_h)\|_0^2 + \varepsilon^2\|\boldsymbol{\sigma}-\boldsymbol{\sigma}_h\|_0^2 +$

$\varepsilon^2\|\nabla(u-\mathscr{I}^{CL}u_h)\|_0^2+\|u-\mathscr{I}^{CL}u_h\|_0^2$. As $\boldsymbol{\sigma}=-\nabla u$, we expect that $\varepsilon^2\|\boldsymbol{\sigma}-\boldsymbol{\sigma}_h\|_0^2$ and $\varepsilon^2\|\nabla(u-\mathscr{I}^{CL}u_h)\|_0^2$ are of the same order of magnitude, i.e., these terms in our estimators are balanced.

We also derive the following guaranteed upper bounds for the quantities of interest that can be used as a stopping criterion to yield any desired accuracy in an adaptive algorithm. For the flux variable, in Theorem 4.1 we obtain

$$\begin{aligned}\|\varepsilon(\boldsymbol{\sigma}-\boldsymbol{\sigma}_h)\|_0^2+\left\|\varepsilon^2\sqrt{b}\,\nabla\cdot(\boldsymbol{\sigma}-\boldsymbol{\sigma}_h)\right\|_0^2\\ \leq\min_{v\in H_0^1(\Omega)}\frac{1}{b_{\min}}\left\|b\,f-\varepsilon^2 b\,\nabla\cdot\boldsymbol{\sigma}_h-v\|_0^2+\varepsilon^2\|\boldsymbol{\sigma}_h+\nabla v\right\|_0^2,\end{aligned}$$

while for the primary approximation, in Theorem 4.2 we show that

$$\begin{aligned}\|u-u_h\|_0\leq\|bf-P_h(bf)\|_0+\varepsilon^2\,\|(b\nabla\cdot\boldsymbol{\sigma}_h-P_h(b\nabla\cdot\boldsymbol{\sigma}_h)\|_0\\ +\min_{v\in H_0^1(\Omega)}\left(\frac{b_{\max}}{b_{\min}}\left\|bf-\varepsilon^2 b\nabla\cdot\boldsymbol{\sigma}_h-v\right\|_0^2+\varepsilon^2\,\frac{b_{\max}}{2}\,\|\boldsymbol{\sigma}_h+\nabla v\|_0^2\right)^{1/2}.\end{aligned}$$

Taking $v=\mathscr{I}^{CL}u_h$ in these two estimates, our numerical examples show that both estimates provide upper bounds that are close to the actual errors. Note that they do not contain any unknown constants, so for any particular choice of $v\in H_0^1(\Omega)$ they can in principle be evaluated very accurately.

Remark 1.2 Parts of our analysis bear a superficial resemblance to the well-known Prager-Synge identity [18], which has been used (see, e.g., [8, 19, 25] and their references) to develop a posteriori error estimates for elliptic problems. This approach requires the underlying numerical method to be locally conservative, which is true for example of mixed finite element methods; it then delivers a posteriori error estimates in which $\|\boldsymbol{\sigma}_h+\nabla v\|$ plays a crucial role. This term appears frequently in the analysis of methods that are related to a least-squares approach. It plays a major role in our analysis (as we saw above), but our numerical method is not locally conservative, and to derive our results via the Prager-Synge identity takes more effort than the relatively simple and straightforward structure of much of our analysis.

The paper is organised as follows. Section 2 describes the setting and formulation of the dual FEM from [5], together with some basic error estimates. In Sect. 3, a posteriori error estimates are derived. Then sharp upper bounds for the primary and flux approximation errors are proved in Sect. 4. Numerical examples that illustrate the sharpness and effectiveness of our results are provided in Sect. 5.

2 The dual FEM and a priori error bounds

In this section we describe the dual FEM of [5] and state the main error bounds derived in [5].

2.1 Dual formulation of (1.1)

The dual formulation of (1.1) is standard and can be found for example in [13]. We now outline this theory.

The minimisation problem corresponding to (1.1) is: find $u \in H_0^1(\Omega)$ such that $J(u) = \inf_{v \in H_0^1(\Omega)} J(v)$, where $J(v)$ is the energy functional defined by

$$J(v) = \frac{1}{2}\left(\varepsilon^2 \|\nabla v\|_0^2 + \left\|b^{-1/2} v\right\|_0^2\right) - (f, v),$$

where $(\cdot, \cdot)$ denotes the $L_2(\Omega)$ inner product. The dual problem of this minimisation problem is: find $\boldsymbol{\sigma} \in H(\mathrm{div})$ such that $J^*(\boldsymbol{\sigma}) = \sup_{\boldsymbol{\tau} \in H(\mathrm{div})} J^*(\boldsymbol{\tau})$, where

$$J^*(\boldsymbol{\tau}) = -\frac{1}{2}\left(\varepsilon^2 \|\boldsymbol{\tau}\|_0^2 + \left\|b^{1/2}(\varepsilon^2 \nabla \cdot \boldsymbol{\tau} - f)\right\|_0^2\right).$$

Then $J(u) = J^*(\boldsymbol{\sigma})$ and $\boldsymbol{\sigma} = -\nabla u$.

The variational problem of the dual problem is: find $\boldsymbol{\sigma} \in H(\mathrm{div})$ such that

$$B(\boldsymbol{\sigma}, \boldsymbol{\tau}) = f(\boldsymbol{\tau}) \quad \forall \boldsymbol{\tau} \in H(\mathrm{div}), \tag{2.1}$$

where $B(\boldsymbol{\sigma}, \boldsymbol{\tau}) := \varepsilon^2 (b \nabla \cdot \boldsymbol{\sigma}, \nabla \cdot \boldsymbol{\tau}) + (\boldsymbol{\sigma}, \boldsymbol{\tau})$ and $f(\boldsymbol{\tau}) := (bf, \nabla \cdot \boldsymbol{\tau})$.

2.2 Finite element spaces

To approximate the solution of (2.1), let $\mathscr{T}_h$ be a partition of Ω into triangles or simplices using a geometrically conformal mesh [14, Section 1.3.3]. Let h_K be the diameter of element $K \in \mathscr{T}_h$ and let $h = \max_{K \in \mathscr{T}_h} h_K$. For each element K, let $P_j(K)$ be the space of polynomials of degree at most j defined on K.

To solve (2.1) numerically, we use a mixed finite element method. To approximate the flux $\boldsymbol{\sigma}$, choose a finite element space $\mathbf{V}_h \subset H(\mathrm{div})$; for some integer $k \geq 0$, one could use the Raviart-Thomas (RT) element of order k or the Brezzi-Douglas-Marini (BDM) element of order $k+1$ (see [4] for details). Then to approximate u, choose a standard FEM space $Q_h \subset L_2(\Omega)$ with $Q_h|_K \supseteq P_j(K)$ for each $K \in \mathscr{T}_h$, where $j = k$ for the RT elements and $j = k+1$ for the BDM elements.

Let $P_h : L_2(\Omega) \to Q_h$ be the local L_2 projection defined by

$$(v - P_h v, q_h) = 0 \quad \forall q_h \in Q_h. \tag{2.2}$$

From [4, Section III.3.4] there exists an interpolant $\Pi_h : H(\mathrm{div}) \to \mathbf{V}_h$ satisfying the commuting diagram property $\nabla \cdot \Pi_h \boldsymbol{\tau} = P_h \nabla \cdot \boldsymbol{\tau}$ for all $\boldsymbol{\tau} \in H(\mathrm{div})$. This property and (2.2) yield

$$(\nabla \cdot (\boldsymbol{\tau} - \Pi_h \boldsymbol{\tau}),\ v_h) = (\nabla \cdot \boldsymbol{\tau} - P_h \nabla \cdot \boldsymbol{\tau}, v_h) = 0 \quad \forall v_h \in Q_h. \tag{2.3}$$

Remark 2.1 Our analysis in this paper can be extended to all mixed-type finite element spaces that possess the above properties. In fact, the development of our a posteriori error estimators does not require the commuting diagram property. However, it is required for a priori error estimates for the dual finite element methods.

We shall also use the standard finite element space of globally-continuous piecewise polynomial of degree r, i.e., $S_{h,r} = \{v \in H_0^1(\Omega) : v \in P_r(T)\, \forall T \in \mathscr{T}_h\}$, which enjoys the approximation property $\|u - u_I\|_i \leq Ch^{r+1-i}\|u\|_{r+1}$ for $i = 0, 1$, where u_I is the Scott-Zhang interpolant [21] of u and C is some fixed constant. Here one takes $r = k + 1$ for the RT elements and $r = k + 2$ for the BDM elements.

2.3 The dual FEM: a two-step method

Here we present the numerical method of [5] for approximating the true solution $(\boldsymbol{\sigma}, u) \in H(\mathrm{div}) \times H_0^1(\Omega)$ of (2.1).
Step 1: Compute the dual variable Define an approximate solution $\boldsymbol{\sigma}_h \in \mathbf{V}_h$ for $\boldsymbol{\sigma} = -\nabla u$ in (2.1) by

$$B(\boldsymbol{\sigma}_h, \boldsymbol{\tau}_h) = (b\, f, \nabla \cdot \boldsymbol{\tau}_h) \quad \forall \boldsymbol{\tau} \in \mathbf{V}_h. \tag{2.4}$$

Step 2: Recover the primary variable The primary approximation is then recovered by a simple local L_2 projection:

$$u_h := P_h\left(b\left(f - \varepsilon^2 \nabla \cdot \boldsymbol{\sigma}_h\right)\right) \in Q_h. \tag{2.5}$$

2.4 A priori error estimates

We now state a priori error estimates for the numerical method defined in (2.4) and (2.5). Note that they do not contain any unknown constants.

Theorem 2.1 [5, Theorem 4.1] *Let $\boldsymbol{\sigma}$ and $\boldsymbol{\sigma}_h$ be the solutions of* (2.1) *and* (2.4) *respectively. Then*

$$\left(\|\boldsymbol{\sigma} - \boldsymbol{\sigma}_h\|_0^2 + \varepsilon^2 \|b^{1/2}\nabla \cdot (\boldsymbol{\sigma} - \boldsymbol{\sigma}_h)\|_0^2\right)^{1/2} \leq \min_{\boldsymbol{\tau}_h \in \mathbf{V}_h} \left(\|\boldsymbol{\sigma} - \boldsymbol{\tau}_h\|_0^2 + \varepsilon^2 \|b^{1/2}\nabla \cdot (\boldsymbol{\sigma} - \boldsymbol{\tau}_h)\|_0^2\right)^{1/2}.$$

Theorem 2.2 [5, Theorem 4.4] *Let u and u_h be the solutions of* (1.1) *and* (2.5) *respectively. Then*

$$\|u - u_h\|_0 \leq \|u - P_h u\|_0 + \varepsilon\sqrt{b_{\max}} \min_{\boldsymbol{\tau}_h \in \mathbf{V}_h} \left(\|\boldsymbol{\sigma} - \boldsymbol{\tau}_h\|_0^2 + \varepsilon^2 \|b^{1/2}\nabla \cdot (\boldsymbol{\sigma} - \boldsymbol{\tau}_h)\|_0^2\right)^{1/2}.$$

Remark 2.2 The quantity $b_{\max}$ will appear several times in our analysis. This is natural—one cannot allow b to be unbounded. If one takes the formal limit $b \to \infty$

in (1.1), this produces the problem $-\varepsilon^2\triangle u = f$ with $u = 0$ on $\partial\Omega$ which has extremely poor stability properties; for instance in 1D with $\Omega = (0, 1)$ and $f \equiv 1$, the solution is $u(x) = x(1 - x)/(2\varepsilon^2)$ which is unbounded as $\varepsilon \to 0$.

3 Reliability and efficiency of the a posteriori error estimator (1.4)

First, we prove that the least-squares functional defined in (1.3) is equivalent to the energy-type norm defined in (1.2) — without any unknown constants appearing in the estimates. This result will immediately imply the reliability and efficiency of our error estimator (1.4).

Lemma 3.1 (Reliability and efficiency of $\eta(\cdot,\cdot)$) *Let* $(\boldsymbol{\tau}, v) \in H(\mathrm{div}) \times H_0^1(\Omega)$ *be arbitrary. Then one has*

$$\frac{1}{2}\eta^2(\boldsymbol{\tau}, v) \le |||(\boldsymbol{\tau}, v)|||^2 \le \left(3\,\frac{\max\{1, b_{\max}\}}{\min\{1, b_{\min}\}} + 2\right)\eta^2(\boldsymbol{\tau}, v), \tag{3.1}$$

where $|||(\boldsymbol{\tau}, v)|||$ *and* $\eta(\boldsymbol{\tau}, v)$ *were defined in* (1.2) *and* (1.4) *respectively.*

Furthermore, in the special case $b \equiv 1$ *one has* $\eta^2(\boldsymbol{\tau}, v) = |||(\boldsymbol{\tau}, v)|||^2$.

Proof Using the definition of η and the Cauchy-Schwarz inequality, we get

$$\begin{aligned}
\eta^2(\boldsymbol{\tau}, v) &= \|\varepsilon\, b\nabla\cdot\boldsymbol{\tau} + v\|_0^2 + \|\boldsymbol{\tau} + \varepsilon\nabla v\|_0^2 \\
&= (\varepsilon\, b\nabla\cdot\boldsymbol{\tau} + v, \varepsilon\, b\nabla\cdot\boldsymbol{\tau} + v) + (\boldsymbol{\tau} + \varepsilon\nabla v, \boldsymbol{\tau} + \varepsilon\nabla v) \\
&= (\varepsilon\, b\nabla\cdot\boldsymbol{\tau}, \varepsilon\, b\nabla\cdot\boldsymbol{\tau}) + (v, v) + (\boldsymbol{\tau}, \boldsymbol{\tau}) + (\varepsilon\nabla v, \varepsilon\nabla v) \\
&\quad + 2(\varepsilon\, b\nabla\cdot\boldsymbol{\tau}, v) + 2(\boldsymbol{\tau}, \varepsilon\nabla v) \\
&\le \|\varepsilon\, b\nabla\cdot\boldsymbol{\tau}\|_0^2 + \|v\|_0^2 + \|\boldsymbol{\tau}\|_0^2 + \|\varepsilon\nabla v\|_0^2 + 2\|\varepsilon\, b\nabla\cdot\boldsymbol{\tau}\|_0\|v\|_0 + 2\|\boldsymbol{\tau}\|_0\|\varepsilon\nabla v\|_0 \\
&\le 2|||(\boldsymbol{\tau}, v)|||^2,
\end{aligned} \tag{3.2}$$

using $2cd \le c^2 + d^2$ twice; the first inequality in (3.1) is now proved.

To establish the reliability of η, i.e., the second inequality in (3.1), note first that

$$\|\phi\|_0^2 \le (\|\phi + \psi\|_0 + \|-\psi\|_0)^2 \le 2\left(\|\phi + \psi\|_0^2 + \|\psi\|_0^2\right)\ \forall \phi, \psi \in L_2(\Omega).$$

Appealing to the definition of $|||(\boldsymbol{\tau}, v)|||$ and applying the above inequality, we obtain

$$\begin{aligned}
|||(\boldsymbol{\tau}, v)|||^2 &= \|\varepsilon\, b\nabla\cdot\boldsymbol{\tau}\|_0^2 + \|\boldsymbol{\tau}\|_0^2 + \|\varepsilon\nabla v\|_0^2 + \|v\|_0^2 \\
&\le \|\varepsilon\, b\nabla\cdot\boldsymbol{\tau}\|_0^2 + \|\boldsymbol{\tau}\|_0^2 \\
&\quad + 2\left(\|\boldsymbol{\tau} + \varepsilon\nabla v\|_0^2 + \|\boldsymbol{\tau}\|_0^2 + \|\varepsilon b\nabla\cdot\boldsymbol{\tau} + v\|_0^2 + \|\varepsilon\, b\nabla\cdot\boldsymbol{\tau}\|_0^2\right) \\
&= 3\left(\|\varepsilon\, b\nabla\cdot\boldsymbol{\tau}\|_0^2 + \|\boldsymbol{\tau}\|_0^2\right) + 2\,\eta^2(\boldsymbol{\tau}, v) \\
&\le 3\max\{1, b_{\max}\}\left(\left\|\varepsilon\sqrt{b}\,\nabla\cdot\boldsymbol{\tau}\right\|_0^2 + \|\boldsymbol{\tau}\|_0^2\right) + 2\,\eta^2(\boldsymbol{\tau}, v).
\end{aligned} \tag{3.3}$$

Using integration by parts, some Cauchy-Schwarz inequalities, and the inequality $cd \le (c^2 + d^2)/2$, one sees that

$$\begin{aligned}
&\left\|\varepsilon\sqrt{b}\,\nabla\cdot\boldsymbol{\tau}\right\|_0^2 + \|\boldsymbol{\tau}\|_0^2 = (\varepsilon b\,\nabla\cdot\boldsymbol{\tau}, \varepsilon\nabla\cdot\boldsymbol{\tau}) + (\boldsymbol{\tau},\boldsymbol{\tau}) \\
&\quad = (\varepsilon b\,\nabla\cdot\boldsymbol{\tau} + v, \varepsilon\nabla\cdot\boldsymbol{\tau}) + (\boldsymbol{\tau} + \varepsilon\nabla v, \boldsymbol{\tau}) \\
&\quad \le \|\varepsilon b\,\nabla\cdot\boldsymbol{\tau} + v\|_0 \|\varepsilon\nabla\cdot\boldsymbol{\tau}\|_0 + \|\boldsymbol{\tau} + \varepsilon\nabla v\|_0 \|\boldsymbol{\tau}\|_0 \\
&\quad \le \frac{1}{\sqrt{b_{\min}}} \|\varepsilon b\,\nabla\cdot\boldsymbol{\tau} + v\|_0 \|\varepsilon\sqrt{b}\,\nabla\cdot\boldsymbol{\tau}\|_0 + \|\boldsymbol{\tau} + \varepsilon\nabla v\|_0 \|\boldsymbol{\tau}\|_0 \\
&\quad \le \frac{1}{2}\left(\frac{1}{b_{\min}}\|\varepsilon b\,\nabla\cdot\boldsymbol{\tau} + v\|_0^2 + \|\boldsymbol{\tau} + \varepsilon\nabla v\|_0^2\right) + \frac{1}{2}\left(\left\|\varepsilon\sqrt{b}\,\nabla\cdot\boldsymbol{\tau}\right\|_0^2 + \|\boldsymbol{\tau}\|_0^2\right).
\end{aligned}$$

Hence

$$\left\|\varepsilon\sqrt{b}\nabla\cdot\boldsymbol{\tau}\right\|_0^2 + \|\boldsymbol{\tau}\|_0^2 \le \frac{1}{b_{\min}}\|\varepsilon b\nabla\cdot\boldsymbol{\tau} + v\|_0^2 + \|\boldsymbol{\tau} + \varepsilon\nabla v\|_0^2 \le \frac{1}{\min\{1, b_{\min}\}}\eta^2(\boldsymbol{\tau}, v).$$

Substituting this inequality into (3.3) yields

$$|||(\boldsymbol{\tau}, v)|||^2 \le \left(3\frac{\max\{1, b_{\max}\}}{\min\{1, b_{\min}\}} + 2\right)\eta^2(\boldsymbol{\tau}, v).$$

This completes the proof of (3.1).

In the special case where $b \equiv 1$, observe that $2(\varepsilon\, b\,\nabla\cdot\boldsymbol{\tau}, v) + 2(\boldsymbol{\tau}, \varepsilon\nabla v) = 0$ in (3.2), and one then obtains $\eta^2(\boldsymbol{\tau}, v) = |||(\boldsymbol{\tau}, v)|||^2$. □

Lemma 3.1 implies immediately the following reliability and efficiency result for the error estimator (1.4).

Theorem 3.1 *Let u be the solution of (1.1), with $\boldsymbol{\sigma} = -\nabla u$ the solution of (2.1). Let $(\boldsymbol{\sigma}_h, u_h)$ be the solution computed by the dual FEM of* Sect. 2.3. *Then*

$$\begin{aligned}
\frac{1}{2}\eta^2\left(\varepsilon(\boldsymbol{\sigma} - \boldsymbol{\sigma}_h), u - \mathscr{I}^{CL}u_h\right) &\le \left|\!\left|\!\left|\left(\varepsilon(\boldsymbol{\sigma} - \boldsymbol{\sigma}_h), u - \mathscr{I}^{CL}u_h\right)\right|\!\right|\!\right|^2 \\
&\le \left(3\frac{\max\{1, b_{\max}\}}{\min\{1, b_{\min}\}} + 2\right)\eta^2\left(\varepsilon(\boldsymbol{\sigma} - \boldsymbol{\sigma}_h), u - \mathscr{I}^{CL}u_h\right).
\end{aligned}$$

Furthermore, in the special case $b \equiv 1$ one has

$$\left|\!\left|\!\left|\left(\varepsilon(\boldsymbol{\sigma} - \boldsymbol{\sigma}_h), u - \mathscr{I}^{CL}u_h\right)\right|\!\right|\!\right| = \eta\left(\varepsilon(\boldsymbol{\sigma} - \boldsymbol{\sigma}_h), u - \mathscr{I}^{CL}u_h\right). \tag{3.4}$$

Proof Chose $\boldsymbol{\tau} = \varepsilon(\boldsymbol{\sigma} - \boldsymbol{\sigma}_h)$ and $v = u - \mathscr{I}^{CL}u_h$ in Lemma 3.1. □

Remark 3.1 We use the Clément interpolant $\mathscr{I}^{CL}u_h$ since it lies in $H_0^1(\Omega)$, it can be computed efficiently from u_h, and it yields excellent numerical results in our numerical experiments (see Sect. 5). But other choices are also possible, such as the Scott-Zhang interpolant [21].

Remark 3.2 For each $T \in \mathscr{T}_h$, define a local analogue of (1.3):

$$\eta_T^2(\boldsymbol{\tau}, v) := \|\varepsilon\, b\, \nabla\cdot\boldsymbol{\tau} + v\|_{0,T}^2 + \|\boldsymbol{\tau} + \varepsilon\nabla v\|_{0,T}^2 \quad \forall(\boldsymbol{\tau}, v) \in H(\mathrm{div}) \times H_0^1(\Omega),$$

where $\|\cdot\|_{0,T}$ is the $L_2(T)$ norm. Then the corresponding local a posteriori error estimator $\eta_T\left(\varepsilon(\boldsymbol{\sigma} - \boldsymbol{\sigma}_h), u - \mathscr{I}^{CL}u_h\right)$ satisfies the following local efficiency bound:

$$\begin{aligned}
&\eta_T^2\left(\varepsilon(\boldsymbol{\sigma} - \boldsymbol{\sigma}_h), u - \mathscr{I}^{CL}u_h\right)\\
&= \left\|\varepsilon\, b\,\nabla\cdot(\varepsilon(\boldsymbol{\sigma} - \boldsymbol{\sigma}_h)) + u - \mathscr{I}^{CL}u_h\right\|_{0,T}^2 + \left\|\varepsilon(\boldsymbol{\sigma} - \boldsymbol{\sigma}_h) + \varepsilon\nabla(u - \mathscr{I}^{CL}u_h)\right\|_{0,T}^2\\
&\le 2\Big(\|\varepsilon\, b\,\nabla\cdot(\varepsilon(\boldsymbol{\sigma} - \boldsymbol{\sigma}_h)\|_{0,T}^2 + \|\varepsilon(\boldsymbol{\sigma} - \boldsymbol{\sigma}_h)\|_{0,T}^2\\
&\quad + \left\|\varepsilon\nabla(u - \mathscr{I}^{CL}u_h)\right\|_{0,T}^2 + \left\|u - \mathscr{I}^{CL}u_h\right\|_{0,T}^2\Big),
\end{aligned}$$

by virtue of a triangle inequality.

4 Guaranteed upper bounds for errors in the primary and dual variables

In this section we shall derive guaranteed upper bounds for the errors in the computed approximations of the dual and primary variables.

Theorem 3.1 already implies crude a posteriori upper bounds for the errors in the computed approximations of the dual and primary variables. We shall improve these upper bounds by considering separately the dual and primary approximations.

4.1 Upper bound for the dual variable error

For the energy-type norm for the error of the dual variables, we show that the error is bounded by a minimum taken over all $v \in H^1(\Omega)$. First, define a norm $|||\cdot|||_d$ on the scaled dual variable error $\varepsilon(\boldsymbol{\sigma} - \boldsymbol{\sigma}_h)$ by

$$|||\varepsilon(\boldsymbol{\sigma} - \boldsymbol{\sigma}_h)|||_d^2 = \|\varepsilon(\boldsymbol{\sigma} - \boldsymbol{\sigma}_h)\|_0^2 + \|\varepsilon^2\sqrt{b}\,\nabla\cdot(\boldsymbol{\sigma} - \boldsymbol{\sigma}_h)\|_0^2. \tag{4.1}$$

Theorem 4.1 *Let u be the solution of (1.1), with $\boldsymbol{\sigma} = -\nabla u$ the solution of (2.1). Let $(\boldsymbol{\sigma}_h, u_h)$ be the solution computed by the dual FEM of* Sect. 2.3. *Then*

$$|||\varepsilon(\boldsymbol{\sigma} - \boldsymbol{\sigma}_h)|||_d^2 \le \min_{v\in H_0^1(\Omega)}\left(\frac{1}{b_{\min}}\|b\, f - \varepsilon^2\, b\nabla\cdot\boldsymbol{\sigma}_h - v\|_0^2 + \varepsilon^2\|\boldsymbol{\sigma}_h + \nabla v\|_0^2\right).$$

Proof Let $v \in H_0^1(\Omega)$ be arbitrary. Using integration by parts, $\boldsymbol{\sigma} = -\nabla u$ and (1.1), one gets

$$\|\boldsymbol{\sigma} - \boldsymbol{\sigma}_h\|_0^2 + \left\|\varepsilon\sqrt{b}\,\nabla\cdot(\boldsymbol{\sigma} - \boldsymbol{\sigma}_h)\right\|_0^2$$

$$
\begin{aligned}
&= (\boldsymbol{\sigma} - \boldsymbol{\sigma}_h\,,\, \boldsymbol{\sigma} - \boldsymbol{\sigma}_h) + \left(\varepsilon^2\, b\nabla\cdot(\boldsymbol{\sigma} - \boldsymbol{\sigma}_h), \nabla\cdot(\boldsymbol{\sigma} - \boldsymbol{\sigma}_h)\right)\\
&= (\boldsymbol{\sigma} - \boldsymbol{\sigma}_h + \nabla(u - v))\,,\, \boldsymbol{\sigma} - \boldsymbol{\sigma}_h) + \left(\varepsilon^2\, b\nabla\cdot(\boldsymbol{\sigma} - \boldsymbol{\sigma}_h) + u - v, \nabla\cdot(\boldsymbol{\sigma} - \boldsymbol{\sigma}_h)\right)\\
&= (-(\boldsymbol{\sigma}_h + \nabla v)\,,\, \boldsymbol{\sigma} - \boldsymbol{\sigma}_h) + \left(b\, f - \varepsilon^2\, b\nabla\cdot\boldsymbol{\sigma}_h - v, \nabla\cdot(\boldsymbol{\sigma} - \boldsymbol{\sigma}_h)\right)\\
&\le \|\boldsymbol{\sigma}_h + \nabla v\|_0 \|\boldsymbol{\sigma} - \boldsymbol{\sigma}_h\|_0 + \frac{1}{\varepsilon\sqrt{b_{\min}}} \left\|b\, f - \varepsilon^2\, b\nabla\cdot\boldsymbol{\sigma}_h - v\right\|_0 \left\|\varepsilon\sqrt{b}\nabla\cdot(\boldsymbol{\sigma} - \boldsymbol{\sigma}_h)\right\|_0 .
\end{aligned}
$$

Applying the inequality $cd \le (c^2 + d^2)/2$ to each product on the right-hand side, then multiplying both sides by ε^2, we obtain the desired result since $v \in H_0^1(\Omega)$ is arbitrary. □

Now choose $v = \mathscr{I}^{CL} u_h \in S_{h,r}$ (for some r) in Theorem 4.1; this yields immediately the following guaranteed upper bound for the error in the computed flux.

Corollary 4.1 *One has*

$$
\begin{aligned}
&|||\varepsilon(\boldsymbol{\sigma} - \boldsymbol{\sigma}_h)|||_d\\
&\quad \le \left(\frac{1}{b_{\min}} \|b\, f - \varepsilon^2\, b\nabla\cdot\boldsymbol{\sigma}_h - \mathscr{I}^{CL} u_h\|_0^2 + \varepsilon^2 \|\boldsymbol{\sigma}_h + \nabla\mathscr{I}^{CL} u_h\|_0^2\right)^{1/2}.
\end{aligned}
$$

Remark 4.1 The reliability estimate of Corollary 4.1 is better than the bound of Theorem 3.1 because it has a smaller constant factor. Consider for example $b \equiv 2$; then Corollary 4.1 gives

$$
\|\varepsilon(\boldsymbol{\sigma} - \boldsymbol{\sigma}_h)\|_0 \le \left(\frac{1}{2} \left\|2f - 2\varepsilon^2\nabla\cdot\boldsymbol{\sigma}_h - \mathscr{I}^{CL} u_h\right\|_0^2 + \varepsilon^2 \left\|\boldsymbol{\sigma}_h + \nabla\mathscr{I}^{CL} u_h\right\|_0^2\right)^{1/2},
$$

while Theorem 3.1 yields

$$
\|\varepsilon(\boldsymbol{\sigma} - \boldsymbol{\sigma}_h)\|_0 \le 2\sqrt{2}\left(\left\|2f - 2\varepsilon^2\nabla\cdot\boldsymbol{\sigma}_h - \mathscr{I}^{CL} u_h\right\|_0^2 + \varepsilon^2 \left\|\boldsymbol{\sigma}_h + \nabla\mathscr{I}^{CL} u_h\right\|_0^2\right)^{1/2}.
$$

4.2 Upper bound for the primary variable error

To derive an upper bound for the primary variable error $\|u - u_h\|_0$, start from the following identity:

$$
\begin{aligned}
u - u_h &= b\, f - P_h(b\, f) - \varepsilon^2\,(b\,\nabla\cdot\boldsymbol{\sigma} - P_h(b\,\nabla\cdot\boldsymbol{\sigma}_h))\\
&= b\, f - P_h(b\, f) - \varepsilon^2 b\,\nabla\cdot(\boldsymbol{\sigma} - \boldsymbol{\sigma}_h) - \varepsilon^2(b\,\nabla\cdot\boldsymbol{\sigma}_h - P_h(b\,\nabla\cdot\boldsymbol{\sigma}_h)). \quad (4.2)
\end{aligned}
$$

Note that the first and third terms on the right-hand side can be evaluated exactly. For the second term, one has the following estimate.

Lemma 4.1 *Let u be the solution of (1.1), with $\boldsymbol{\sigma} = -\nabla u$ the solution of (2.1). Let $(\boldsymbol{\sigma}_h, u_h)$ be the solution computed by the dual FEM of* Sect. 2.3. *Then*

$$\varepsilon^2 \|b\,\nabla\cdot(\boldsymbol{\sigma}-\boldsymbol{\sigma}_h)\|_0 \leq \min_{v\in H_0^1(\Omega)} \left(\frac{b_{\max}}{b_{\min}} \|bf - \varepsilon^2 b\,\nabla\cdot\boldsymbol{\sigma}_h - v\|_0^2 + \varepsilon^2\,\frac{b_{\max}}{2}\|\boldsymbol{\sigma}_h + \nabla v\|_0^2 \right)^{1/2}.$$

Proof Clearly

$$\varepsilon^2\|b\nabla\cdot(\boldsymbol{\sigma}-\boldsymbol{\sigma}_h)\|_0 \leq \left(\varepsilon\sqrt{b_{\max}}\right)\varepsilon\left\|\sqrt{b}\,\nabla\cdot(\boldsymbol{\sigma}-\boldsymbol{\sigma}_h)\right\|_0. \tag{4.3}$$

Let $v \in H_0^1(\Omega)$ be arbitrary. Using integration by parts, $\boldsymbol{\sigma} = -\nabla u$ and (1.1), and Cauchy-Schwarz inequalities, we obtain

$$\begin{aligned}
&\varepsilon^2\left\|\sqrt{b}\,\nabla\cdot(\boldsymbol{\sigma}-\boldsymbol{\sigma}_h)\right\|_0^2 \\
&= \left(\varepsilon^2 b\nabla\cdot(\boldsymbol{\sigma}-\boldsymbol{\sigma}_h),\,\nabla\cdot(\boldsymbol{\sigma}-\boldsymbol{\sigma}_h)\right) \\
&= \left(\varepsilon^2 b\nabla\cdot(\boldsymbol{\sigma}-\boldsymbol{\sigma}_h)+u-v,\,\nabla\cdot(\boldsymbol{\sigma}-\boldsymbol{\sigma}_h)\right) + \left(\nabla(u-v)\,,\,\boldsymbol{\sigma}-\boldsymbol{\sigma}_h\right) \\
&= \left(\varepsilon^2 b\nabla\cdot(\boldsymbol{\sigma}-\boldsymbol{\sigma}_h)+u-v,\,\nabla\cdot(\boldsymbol{\sigma}-\boldsymbol{\sigma}_h)\right) \\
&\quad + \left(\nabla(u-v)\,,\,\boldsymbol{\sigma}-\boldsymbol{\sigma}_h+\nabla(u-v)\right) - \|\nabla(u-v)\|_0^2 \\
&\leq \left\|\frac{1}{\sqrt{b}}\left(bf-\varepsilon^2 b\nabla\cdot\boldsymbol{\sigma}_h - v\right)\right\|_0 \left\|\sqrt{b}\,\nabla\cdot(\boldsymbol{\sigma}-\boldsymbol{\sigma}_h)\right\|_0 \\
&\qquad + \|\nabla(u-v)\|_0\,\|\boldsymbol{\sigma}_h+\nabla v\|_0 - \|\nabla(u-v)\|_0^2 \\
&\leq \frac{1}{2\varepsilon^2\,b_{\min}}\left\|bf-\varepsilon^2 b\nabla\cdot\boldsymbol{\sigma}_h - v\right\|_0^2 + \frac{\varepsilon^2}{2}\left\|\sqrt{b}\nabla\cdot(\boldsymbol{\sigma}-\boldsymbol{\sigma}_h)\right\|_0^2 + \frac{1}{4}\|\boldsymbol{\sigma}_h+\nabla v\|_0^2,
\end{aligned}$$

where we also used Young's inequality for products in the forms $cd \leq c^2/(2\varepsilon^2) + \varepsilon^2 d^2/2$ and $cd \leq c^2 + d^2/4$. Hence

$$\varepsilon^2\left\|\sqrt{b}\,\nabla\cdot(\boldsymbol{\sigma}-\boldsymbol{\sigma}_h)\right\|_0^2 \leq \frac{1}{\varepsilon^2 b_{\min}}\left\|bf-\varepsilon^2 b\,\nabla\cdot\boldsymbol{\sigma}_h - v\right\|_0^2 + \frac{1}{2}\|\boldsymbol{\sigma}_h+\nabla v\|_0^2.$$

Substituting this bound into (4.3) yields the result of the lemma. □

It is now easy to prove the following guaranteed upper bound for the error $\|u-u_h\|_0$.

Theorem 4.2 *Let u be the solution of (1.1), with $\boldsymbol{\sigma} = -\nabla u$ the solution of (2.1). Let $(\boldsymbol{\sigma}_h, u_h)$ be the solution computed by the dual FEM of* Sect. 2.3. *Then*

$$\begin{aligned}
\|u-u_h\|_0 \leq{}& \|bf - P_h(bf)\|_0 + \varepsilon^2\,\|(b\nabla\cdot\boldsymbol{\sigma}_h - P_h(b\nabla\cdot\boldsymbol{\sigma}_h)\|_0 \\
&+ \min_{v\in H_0^1(\Omega)}\left(\frac{b_{\max}}{b_{\min}}\left\|bf-\varepsilon^2 b\nabla\cdot\boldsymbol{\sigma}_h - v\right\|_0^2 + \varepsilon^2\,\frac{b_{\max}}{2}\|\boldsymbol{\sigma}_h+\nabla v\|_0^2\right)^{1/2}.
\end{aligned}$$

Proof Combine (4.2) and Lemma 4.1. □

Corollary 4.2 *One has*

$$\|u-u_h\|_0 \le \|bf - P_h(bf)\|_0 + \varepsilon^2 \|b\nabla\cdot\boldsymbol{\sigma}_h - P_h(b\nabla\cdot\boldsymbol{\sigma}_h)\|_0 + \left(\frac{b_{\max}}{b_{\min}}\left\|b\,f - \varepsilon^2 b\nabla\cdot\boldsymbol{\sigma}_h - \mathscr{I}^{CL}u_h\right\|_0^2 + \varepsilon^2\,\frac{b_{\max}}{2}\left\|\boldsymbol{\sigma}_h + \nabla\mathscr{I}^{CL}u_h\right\|_0^2\right)^{1/2}.$$

Proof Choose $v = \mathscr{I}^{CL}u_h$ in Theorem 4.2. □

4.3 A guaranteed energy-norm a posteriori bound for $u - \mathscr{I}^{CL}u_h$

Define the energy-type norm

$$|||v|||_e := \left(\|v\|_0^2 + \varepsilon^2\left\|\sqrt{b}\,\nabla v\right\|_0^2\right)^{1/2} \quad \forall v \in H_0^1(\Omega). \tag{4.4}$$

The recovered solution $\mathscr{I}^{CL}u_h$ can of course be used as a computable approximation for the primary variable u; in fact, our numerical experiments indicate that $|||u-\mathscr{I}^{CL}u_h|||_e$ is smaller than $\|u-u_h\|_0$ when the mesh is sufficiently refined. Thus in the current section we shall derive a guaranteed a posteriori upper bound for $|||u-\mathscr{I}^{CL}u_h|||_e$.

In fact, our theory here is very general: it can be applied to solutions computed by other FEMs as well as the solution computed by the dual FEM of Sect. 2.3. We begin with the following result.

Theorem 4.3 *Let u be the solution of (1.1), with $\boldsymbol{\sigma} = -\nabla u$ the solution of (2.1). Let $v \in H_0^1(\Omega)$ be arbitrary. Then*

$$|||u-v|||_e^2 \le \min_{\boldsymbol{\tau}\in H(\mathrm{div})}\left(\frac{b_{\max}}{b_{\min}}\left\|b\,f - \varepsilon^2\,b\nabla\cdot\boldsymbol{\tau} - v\right\|_0^2 + \varepsilon^2\left(\frac{b_{\max}}{\sqrt{b_{\min}}}\,\|\boldsymbol{\tau}+\nabla v\|_0\right)^2\right).$$

Proof Fix $v \in H_0^1(\Omega)$. Let $\boldsymbol{\tau} \in H(\mathrm{div})$ be arbitrary. Using integration by parts, Cauchy-Schwarz inequalities, $\boldsymbol{\sigma} = -\nabla u$ and (1.1), we have

$$\begin{aligned}
&\|u-v\|_0^2 + \varepsilon^2\left\|\sqrt{b}\,\nabla(u-v)\right\|_0^2\\
&\le (u-v,u-v) + b_{\max}\varepsilon^2\,(\nabla(u-v),\nabla(u-v))\\
&= (u-v,u-v) + b_{\max}\varepsilon^2\,(\boldsymbol{\sigma}-\boldsymbol{\tau}+\nabla(u-v),\nabla(u-v))\\
&\quad + b_{\max}\left(\varepsilon^2\,b\,\nabla\cdot(\boldsymbol{\sigma}-\boldsymbol{\tau}),\frac{1}{b}(u-v)\right)\\
&\le b_{\max}\left(\varepsilon^2\,b\,\nabla\cdot(\boldsymbol{\sigma}-\boldsymbol{\tau}) + u - v,\frac{1}{b}(u-v)\right)
\end{aligned}$$

$$
\begin{aligned}
&+ b_{\max}\varepsilon^2\,(\boldsymbol{\sigma}-\boldsymbol{\tau}+\nabla(u-v),\nabla(u-v))\\
&\le \frac{b_{\max}}{b_{\min}}\left\|b\,f-\varepsilon^2\,b\nabla\cdot\boldsymbol{\tau}-v\right\|_0\|(u-v)\|_0+\frac{b_{\max}}{\sqrt{b_{\min}}}\,\varepsilon^2\,\|\boldsymbol{\tau}+\nabla v\|_0\left\|\sqrt{b}\,\nabla(u-v)\right\|_0\\
&\le \frac{1}{2}\left(\left(\frac{b_{\max}}{b_{\min}}\left\|b\,f-\varepsilon^2 b\,\nabla\cdot\boldsymbol{\tau}-v\right\|_0\right)^2+\varepsilon^2\left(\frac{b_{\max}}{\sqrt{b_{\min}}}\,\|\boldsymbol{\tau}+\nabla v\|_0\right)^2\right)\\
&\quad+\frac{1}{2}\left(\|u-v\|_0^2+\varepsilon^2\left\|\sqrt{b}\,\nabla(u-v)\right\|_0^2\right),
\end{aligned}
$$

where the inequality $cd \le (c^2+d^2)/2$ was used twice in the final step. After solving for $\|u-v\|_0^2+\varepsilon^2\left\|\sqrt{b}\,\nabla(u-v)\right\|_0^2$, the result follows since $\boldsymbol{\tau}\in H(\mathrm{div})$ was arbitrary. □

We can now give a guaranteed a posteriori upper bound for $\left|\!\left|\!\left|u-\mathscr{I}^{CL}u_h\right|\!\right|\!\right|_e$.

Corollary 4.3 *Let $(\boldsymbol{\sigma}_h,u_h)$ be the solution computed by the dual FEM of* Sect. 2.3. *Let $\mathscr{I}^{CL}u_h\in H_0^1(\Omega)$ be the recovered approximation of u. Then*

$$
\begin{aligned}
&\left|\!\left|\!\left|u-\mathscr{I}^{CL}u_h\right|\!\right|\!\right|_e^2\\
&\le\left(\frac{b_{\max}}{b_{\min}}\left\|b\,f-\varepsilon^2 b\,\nabla\cdot\boldsymbol{\sigma}_h-\mathscr{I}^{CL}u_h\right\|_0\right)^2+\varepsilon^2\left(\frac{b_{\max}}{\sqrt{b_{\min}}}\left\|\boldsymbol{\sigma}_h+\nabla\mathscr{I}^{CL}u_h\right\|_0\right)^2.
\end{aligned}
$$

Proof Choose $v=\mathscr{I}^{CL}u_h$ and $\boldsymbol{\tau}=\boldsymbol{\sigma}_h$ in Theorem 4.3. □

Remark 4.2 Theorem 4.3 also gives a guaranteed upper bound for the error $\left|\!\left|\!\left|u-u_h^G\right|\!\right|\!\right|_e$, where $u_h^G\in H_0^1(\Omega)$ is the solution computed by the standard Galerkin FEM when solving (1.1). One simply chooses $v=u_h^G$ in Theorem 4.3, obtaining

$$
\left|\!\left|\!\left|u-u_h^G\right|\!\right|\!\right|_e^2\le\min_{\boldsymbol{\tau}\in H(\mathrm{div})}\left(\frac{b_{\max}}{b_{\min}}\left\|b\,f-\varepsilon^2\,b\nabla\cdot\boldsymbol{\tau}-u_h^G\right\|_0^2+\varepsilon^2\left(\frac{b_{\max}}{\sqrt{b_{\min}}}\left\|\boldsymbol{\tau}+\nabla u_h^G\right\|_0\right)^2\right).
$$

5 Numerical examples

In this section, we present numerical examples confirming our theoretical results and demonstrating the efficiency and accuracy of our a posteriori error estimators/indicators for the model problem (1.1).

The approximation space $\mathbf{V}_h$ for the flux variables is taken to be RT_0, the lowest-order Raviart-Thomas space, and we use piecewise constants to approximate the primary variable. The space $S_{h,1}$ of globally continuous piecewise linears is used for the recovery $\mathscr{I}^{CL}u_h$ of the primary variable in the error estimators and upper bounds. Integrals are evaluated by means of the 13-point quadrature rule from [23, p.184].

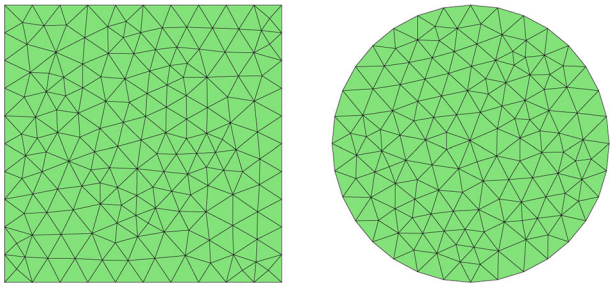

Fig. 1 Initial meshes

5.1 Examples with shape-regular meshes

We consider the problem (1.1) on $\Omega = (0, 1)^2$. The initial meshes in Sect. 5.1 are generated by the MATLAB function "initmesh.m" and displayed in Fig. 1.

The a posteriori error indicator defined in (1.4) will be tested. To compute $\mathscr{I}^{CL}(u_h)$, we use the MATLAB function "recoverP02P1.m" from iFEM [7]. For mesh refinement, Dörfler's marking strategy [11] is used with a bulk parameter 0.7, i.e., our algorithm selects a subset $\mathscr{M}$ of $\mathscr{T}_h$ that satisfies $(0.7)\eta^2 \leq \sum_{T\in\mathscr{M}} \eta_T^2$, where η_T was defined in Remark 3.2, then the MATLAB function "refinemesh.m" is used to refine the current mesh by dividing each specified triangle into four triangles of the same shape.

Define an effectivity index by

$$\text{E-index} = \frac{|||(\varepsilon(\boldsymbol{\sigma} - \boldsymbol{\sigma}_h), u - u_h)|||}{\eta\,(\varepsilon(\boldsymbol{\sigma} - \boldsymbol{\sigma}_h), u - u_h)}.$$

Let $\mathbf{U}(|||\varepsilon(\boldsymbol{\sigma} - \boldsymbol{\sigma}_h)|||_d)$, $\mathbf{U}(\|u - u_h\|_0)$ and $\mathbf{U}(\left|\left|\left|u - \mathscr{I}^{CL}(u_h)\right|\right|\right|_e)$ denote the right-hand sides of Corollaries 4.1, 4.2, and 4.3 respectively. These quantities will be upper bounds for $|||\varepsilon(\boldsymbol{\sigma} - \boldsymbol{\sigma}_h)|||_d$, $\|u - u_h\|_0$, and $\left|\left|\left|u - \mathscr{I}^{CL}(u_h)\right|\right|\right|_e$, where $|||\varepsilon(\boldsymbol{\sigma} - \boldsymbol{\sigma}_h)|||_d$ and $\left|\left|\left|u - \mathscr{I}^{CL}(u_h)\right|\right|\right|_e$ are defined in (4.1) and (4.4).

In the case $b = 1$, $\mathbf{U}(|||\varepsilon(\boldsymbol{\sigma} - \boldsymbol{\sigma}_h)|||_d)$ is the same as $\mathbf{U}(\left|\left|\left|u - \mathscr{I}^{CL}(u_h)\right|\right|\right|_e)$.

Example 5.1 We consider (1.1) on $\Omega = (0, 1)^2$ with true solution

$$u(x, y) = \left(\cos\left(\frac{\pi x}{2}\right) - \frac{e^{-x/\varepsilon} - e^{1/\varepsilon}}{1 - e^{-1/\varepsilon}}\right)\left(1 - y - \frac{e^{-y/\varepsilon} - e^{1/\varepsilon}}{1 - e^{-1/\varepsilon}}\right)$$

for $b \equiv 1$ and $b(x, y) = 2 + \sin(xy)$, and f chosen to satisfy (1.1) in each case. This solution clearly exhibits boundary layers along the sides $x = 0$ and $y = 0$ of Ω. (For greater clarity in Fig. 2 we have chosen an example without layers along the sides $x = 1$ and $y = 1$, but this does not make the problem easier to solve.) Our a posteriori error indicator locates these layers and refines the mesh in these regions, as shown in Fig. 2.

Table 1 Example 5.1: Convergence behavior for $b \equiv 1$ with $\varepsilon = 0.01$

DoFs	488	632	895	1390	2323	4567	10527	26587	79737
E-index	0.9898	0.9974	0.9995	0.9998	1.0000	1.0000	1.0000	1.0000	1.0000
$\|u - u_h\|_0$	0.0523	0.0431	0.0328	0.0244	0.0192	0.0163	0.0150	0.0141	0.0086
$\mathbf{U}(\|u - u_h\|_0)$	0.1483	0.1025	0.0694	0.0488	0.0359	0.0276	0.0224	0.0189	0.0116
$\frac{\mathbf{U}(\|u-u_h\|_0)}{\|u-u_h\|_0}$	2.84	2.38	2.12	2.00	1.87	1.69	1.49	1.34	1.35
$\|\|\|\varepsilon(\boldsymbol{\sigma} - \boldsymbol{\sigma}_h)\|\|\|_d$	0.0657	0.0531	0.0393	0.0273	0.0179	0.0115	0.0073	0.0045	0.0028
$\mathbf{U}(\|\|\|\varepsilon(\boldsymbol{\sigma} - \boldsymbol{\sigma}_h)\|\|\|_d)$	0.1337	0.0908	0.0592	0.0387	0.0250	0.0161	0.0102	0.0064	0.0040
$\frac{\mathbf{U}(\|\|\|\varepsilon(\boldsymbol{\sigma}-\boldsymbol{\sigma}_h)\|\|\|_d)}{\|\|\|\varepsilon(\boldsymbol{\sigma}-\boldsymbol{\sigma}_h)\|\|\|_d}$	2.04	1.71	1.51	1.42	1.40	1.40	1.42	1.42	1.42
$\left\|\left\|\left\|u - \mathscr{I}^{CL}(u_h)\right\|\right\|\right\|_e$	0.1148	0.0734	0.0442	0.0274	0.0175	0.0113	0.0071	0.0045	0.0028
$\mathbf{U}(\left\|\left\|\left\|u - \mathscr{I}^{CL}(u_h)\right\|\right\|\right\|_e)$	0.1337	0.0908	0.0592	0.0387	0.0250	0.0161	0.0102	0.0064	0.0040
$\frac{\mathbf{U}(\left\|\left\|\left\|u-\mathscr{I}^{CL}(u_h)\right\|\right\|\right\|_e)}{\left\|\left\|\left\|u-\mathscr{I}^{CL}(u_h)\right\|\right\|\right\|_e}$	1.16	1.24	1.34	1.41	1.43	1.42	1.44	1.42	1.42

Table 2 Example 5.1: Convergence behavior for $b(x, y) = 2 + \sin(xy)$ with $\varepsilon = 0.01$

DoFs	488	629	908	1457	2508	4899	11122	26919	71403
E-index	1.0590	1.0411	1.0252	1.0128	1.0058	1.0038	1.0016	1.0008	1.0003
$\|u - u_h\|_0$	0.0604	0.0475	0.0341	0.0243	0.0191	0.0162	0.0150	0.0144	0.0091
$\mathbf{U}(\|u - u_h\|_0)$	0.3055	0.2187	0.1451	0.0950	0.0646	0.0451	0.0333	0.0259	0.0164
$\frac{\mathbf{U}(\|u-u_h\|_0)}{\|u-u_h\|_0}$	5.06	4.60	4.26	3.91	3.38	2.78	2.22	1.80	1.80
$\|\|\|\varepsilon(\boldsymbol{\sigma} - \boldsymbol{\sigma}_h)\|\|\|_d$	0.0827	0.0665	0.0475	0.0320	0.0208	0.0132	0.0085	0.0053	0.0033
$\mathbf{U}(\|\|\|\varepsilon(\boldsymbol{\sigma} - \boldsymbol{\sigma}_h)\|\|\|_d)$	0.1547	0.1101	0.0726	0.0467	0.0302	0.0193	0.0123	0.0078	0.0049
$\frac{\mathbf{U}(\|\|\|\varepsilon(\boldsymbol{\sigma}-\boldsymbol{\sigma}_h)\|\|\|_d)}{\|\|\|\varepsilon(\boldsymbol{\sigma}-\boldsymbol{\sigma}_h)\|\|\|_d}$	1.87	1.66	1.53	1.46	1.45	1.46	1.45	1.47	1.48
$\left\|\left\|\left\|u - \mathscr{I}^{CL}(u_h)\right\|\right\|\right\|_e$	0.1238	0.0841	0.0535	0.0342	0.0225	0.0150	0.0096	0.0062	0.0039
$\mathbf{U}(\left\|\left\|\left\|u - \mathscr{I}^{CL}(u_h)\right\|\right\|\right\|_e)$	0.2598	0.1844	0.1212	0.0777	0.0501	0.0321	0.0204	0.0129	0.0081
$\frac{\mathbf{U}(\left\|\left\|\left\|u-\mathscr{I}^{CL}(u_h)\right\|\right\|\right\|_e)}{\left\|\left\|\left\|u-\mathscr{I}^{CL}(u_h)\right\|\right\|\right\|_e}$	2.10	2.19	2.27	2.27	2.23	2.14	2.13	2.08	2.08

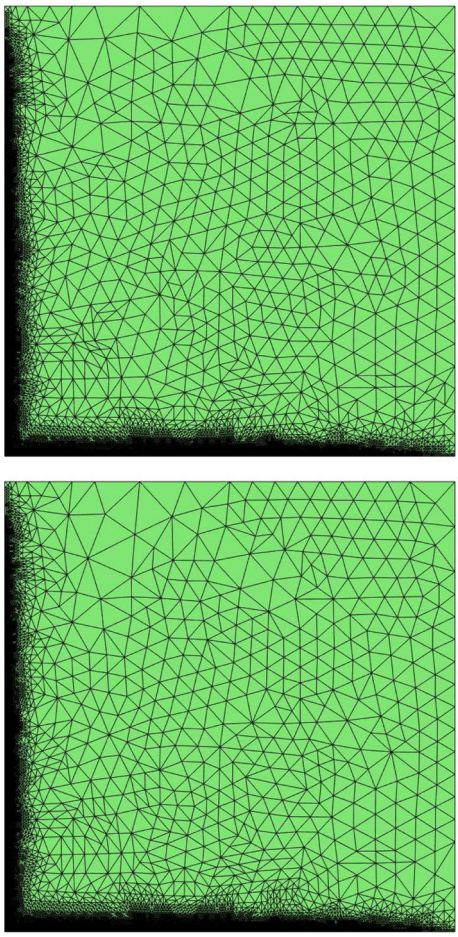

Fig. 2 Meshes generated for Example 5.1 with $\varepsilon = 0.01$. Top: $b \equiv 1$, DoF $= 70737$; Bottom: $b = 2 + \sin(xy)$, DoF $= 71403$

Example 5.2 Consider (1.1) with domain the unit disk $\Omega = \{(x, y) \in \mathbb{R}^2 : x^2 + y^2 < 1\}$ and true solution

$$u(x, y) = \tanh\left(\frac{1}{\varepsilon}\left(x^2 + y^2 - \frac{1}{4}\right)\right) - \tanh\left(\frac{3}{4\varepsilon}\right).$$

This solution has an interior layer along the circle $r = \sqrt{x^2 + y^2} = 1/2$. The mesh generated using our a posteriori error indicator (1.4) locates this interior layer and refines the mesh in its neighborhood; see Fig. 3.

In our numerical experiments the effectivity index is 1 when $b \equiv 1$ (as predicted in (3.4)) and is close to 1 for $b(x, y) = 2+\sin(xy)$. This desirable behavior demonstrates the high quality of our error indicator. Furthermore, the bounds of Corollary 4.1 and 4.2 provide accurate upper bounds for the errors in the approximations computed for the flux and primary variables; see Tables 1, 2, 3 and 4

Table 3 Example 5.2: Convergence behavior for $b = 1$ with $\varepsilon = 0.01$

DoFs	403	682	1387	2887	6358	14710	35086	84781
E-index	1.0344	1.0053	1.0030	0.9998	1.0000	1.0000	1.0000	1.0000
$\|u - u_h\|_0$	0.3945	0.2740	0.1605	0.0908	0.0499	0.0297	0.0196	0.0114
$\mathbf{U}(\|u - u_h\|_0)$	1.0467	0.8240	0.5640	0.3569	0.1963	0.1084	0.0733	0.0434
$\frac{\mathbf{U}(\|u-u_h\|_0}{\|u-u_h\|_0}$	2.65	3.01	3.51	3.93	3.93	3.65	3.74	3.81
$\|\|\|\varepsilon(\boldsymbol{\sigma} - \boldsymbol{\sigma}_h)\|\|\|_d$	0.2729	0.2368	0.1948	0.1397	0.0870	0.0531	0.0350	0.0215
$\mathbf{U}(\|\|\|\varepsilon(\boldsymbol{\sigma} - \boldsymbol{\sigma}_h)\|\|\|_d)$	0.5786	0.4479	0.3167	0.2048	0.1223	0.0742	0.0457	0.0281
$\frac{\mathbf{U}(\|\|\|\varepsilon(\boldsymbol{\sigma}-\boldsymbol{\sigma}_h)\|\|\|_d)}{\|\|\|\varepsilon(\boldsymbol{\sigma}-\boldsymbol{\sigma}_h)\|\|\|_d}$	2.12	1.89	1.63	1.47	1.41	1.40	1.30	1.31
$\left\|\left\|\left\|u - \mathscr{I}^{CL}(u_h)\right\|\right\|\right\|_e$	0.5327	0.3830	0.2509	0.1494	0.0859	0.0518	0.0293	0.0180
$\mathbf{U}(\left\|\left\|\left\|u - \mathscr{I}^{CL}(u_h)\right\|\right\|\right\|_e)$	0.5786	0.4479	0.3167	0.2048	0.1223	0.0742	0.0456	0.0281
$\frac{\mathbf{U}(\left\|\left\|\left\|u-\mathscr{I}^{CL}(u_h)\right\|\right\|\right\|_e)}{\left\|\left\|\left\|u-\mathscr{I}^{CL}(u_h)\right\|\right\|\right\|_e}$	1.09	1.17	1.26	1.37	1.42	1.43	1.56	1.56

Table 4 Example 5.2: Convergence behavior for $b = 1$ with $\varepsilon = 0.001$

DoFs	403	682	1480	2815	5623	11062	22435	47836	105832
E-index	1.0042	0.9984	1.0168	0.9974	0.9950	0.9989	0.9988	1.0001	1.0000
$\|u - u_h\|_0$	0.4373	0.3372	0.2298	0.1644	0.1073	0.0660	0.0371	0.0206	0.0121
$\mathbf{U}(\|u - u_h\|_0)$	1.0318	0.7651	0.5487	0.4046	0.2980	0.2155	0.1394	0.0807	0.0453
$\frac{\mathbf{U}(\|u-u_h\|_0)}{\|u-u_h\|_0}$	2.65	3.01	3.51	3.93	3.93	3.65	3.74	3.81	3.81
$\|\|\|\varepsilon(\boldsymbol{\sigma} - \boldsymbol{\sigma}_h)\|\|\|_d$	0.1040	0.0748	0.0822	0.0817	0.0777	0.0683	0.0518	0.0340	0.0212
$\mathbf{U}(\|\|\|\varepsilon(\boldsymbol{\sigma} - \boldsymbol{\sigma}_h)\|\|\|_d)$	0.5602	0.4168	0.3010	0.2176	0.1608	0.1172	0.0794	0.0489	0.0299
$\frac{\mathbf{U}(\|\|\|\varepsilon(\boldsymbol{\sigma}-\boldsymbol{\sigma}_h)\|\|\|_d)}{\|\|\|\varepsilon(\boldsymbol{\sigma}-\boldsymbol{\sigma}_h)\|\|\|_d}$	5.39	5.57	3.66	2.66	2.07	1.72	1.53	1.44	1.41
$\left\|\left\|\left\|u - \mathscr{I}^{CL}(u_h)\right\|\right\|\right\|_e$	0.5481	0.4107	0.2884	0.2023	0.1417	0.0954	0.0603	0.0351	0.0211
$\mathbf{U}(\left\|\left\|\left\|u - \mathscr{I}^{CL}(u_h)\right\|\right\|\right\|_e)$	0.5602	0.4168	0.3010	0.2176	0.1608	0.1172	0.0794	0.0489	0.0299
$\frac{\mathbf{U}(\left\|\left\|\left\|u-\mathscr{I}^{CL}(u_h)\right\|\right\|\right\|_e)}{\left\|\left\|\left\|u-\mathscr{I}^{CL}(u_h)\right\|\right\|\right\|_e}$	1.02	1.01	1.04	1.07	1.13	1.23	1.32	1.39	1.42

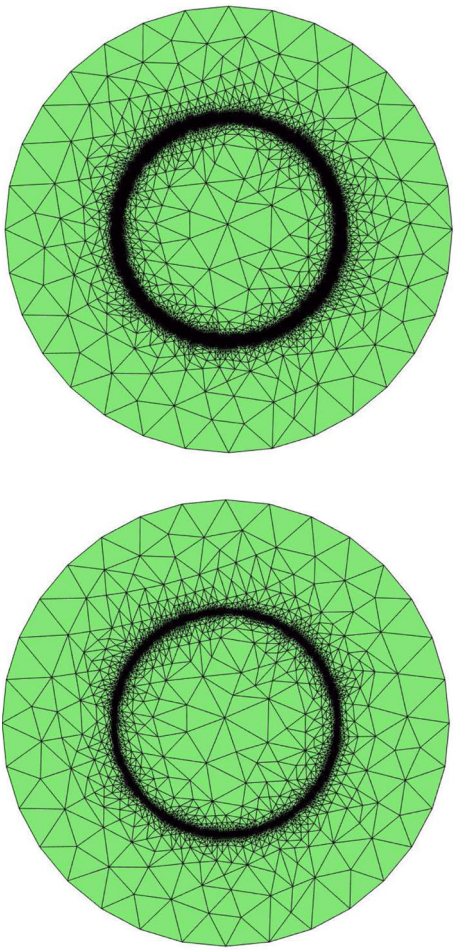

Fig. 3 Meshes generated for Example 5.2. Top $\varepsilon = 0.01$, DoF $= 84781$; Bottom: $\varepsilon = 0.001$, DoF $= 105832$

5.2 Example with anisotropic meshes

The shape-regular meshes of Sect. 5.1 are not the best way to implement an adaptive procedure for problems with boundary layers: long thin anisotropic mesh elements require fewer degrees of freedom to achieve the same accuracy as shape-regular meshes. In a future paper built around numerical experiments we will investigate adaptive procedures that generate anisotropic meshes with mesh elements aligned to the layers in the solution; for the moment, we present a single example to test our error estimators on anisotropic meshes that are specified a priori.

Example 5.3 Consider again Example 5.1 with $\varepsilon = 0.0001$ and $b \equiv 1$.

To solve Example 5.3 numerically, we use the anisotropic meshes of Durán and Lombardi [12]. That is, given a user-chosen parameter $h > 0$, partition the interval

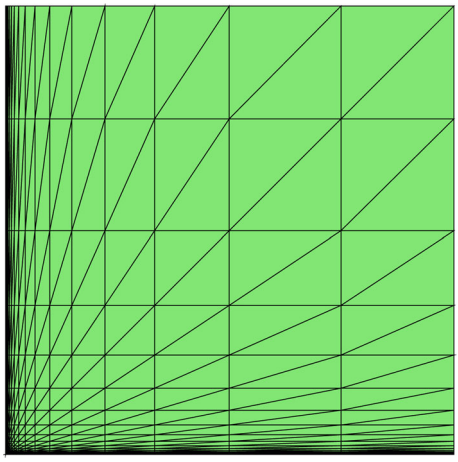

Fig. 4 Anisotropic mesh with $h = 1/2$

$[0, 1]$ by the mesh $\{x_i\}_{i=0}^{M}$, where

$$\begin{cases} x_0 = 0, \\ x_i = ih\varepsilon & \text{for } 1 \le i < \frac{1}{h} + 1, \\ x_{i+1} = x_i + hx_i & \text{for } \frac{1}{h} + 1 \le i \le M - 2, \\ x_M = 1; \end{cases}$$

here M is such that $x_{M-1} < 1$ and $x_{M-1} + hx_{M-1} > 1$. (If the final interval $[x_{M-1}, x_M]$ is too small compared with the previous interval $[x_{M-2}, x_{M-1}]$, then remove x_{M-1}.) Define $y_i = x_i$ for $i = 0, 1, \ldots, M$. Then draw horizontal and vertical lines through the mesh points $\{(x_i, y_j) : i, j = 0, 1, \ldots, M\}$ to partition $\Omega = (0, 1)^2$ into M^2 mesh rectangles. Bisect each mesh rectangle into two triangles by connecting its lower left and upper right corners. Figure 4 shows the mesh obtained when $h = 1/2$; it is clearly highly anisotropic.

In our experiments we took $h = 2^{-1}, 2^{-2}, \ldots, 2^{-5}$. The results are presented in Table 5. The first row of the table shows the maximum mesh aspect ratio for each value of h, to emphasise the anisotropic nature of the mesh. Unlike our examples in Sect. 5.1, the construction of the mesh is not driven by the a posteriori error indicators, so it is unreasonable to expect tight agreement between the actual errors and their computed upper bounds. Nevertheless we find that our error indicators perform reasonably well. The upper bound for $\|u - u_h\|$ given by $\mathbf{U}(\|u - u_h\|)$ in Corollary 4.2 — i.e., choosing $v = \mathscr{I}^{CL} u_h$ in Theorem 4.2 — is however less accurate than in our shape-regular examples. By choosing instead $v = u_h^R$ in Theorem 4.2, where $u_h^R \in S_{h,1}$ is defined by

$$(\nabla u_h^R, \nabla v_h) = (-\boldsymbol{\sigma}_h, \nabla v_h) \; \forall v_h \in S_{h,1},$$

we obtain more accurate upper bounds. Thus, we replace $\mathscr{I}^{CL} u_h$ by u_h^R in the numerical results for this example. As our theory predicts, the E-index is 1 because $b \equiv 1$.

Table 5 Example 5.3: Convergence behavior for $b = 1$ with $\varepsilon = 0.0001$

DoFs	1925 ($h = \frac{1}{2}$)	6165 ($h = \frac{1}{2^2}$)	22360 ($h = \frac{1}{2^3}$)	84001 ($h = \frac{1}{2^4}$)	329345 ($h = \frac{1}{2^5}$)
Max aspect ratio	5.90e+3	9.90e+3	1.05e+4	1.76e+4	1.26e+4
E-index	1.0000	1.0000	1.0000	1.0000	1.000
$\|u - u_h\|_0$	0.0520	0.0405	0.0205	0.0141	0.0079
$\mathbf{U}(\|u - u_h\|_0)$	0.1510	0.1153	0.0727	0.0507	0.0319
$\frac{\mathbf{U}(\|u-u_h\|_0)}{\|u-u_h\|_0}$	2.90	2.85	3.55	3.60	4.04
$\|\|\|\varepsilon(\boldsymbol{\sigma} - \boldsymbol{\sigma}_h)\|\|\|_d$	0.0090	0.0090	0.0089	0.0087	0.0085
$\mathbf{U}(\|\|\|\varepsilon(\boldsymbol{\sigma} - \boldsymbol{\sigma}_h)\|\|\|_d)$	0.994	0.754	0.0532	0.0381	0.0270
$\frac{\mathbf{U}(\|\|\|\varepsilon(\boldsymbol{\sigma}-\boldsymbol{\sigma}_h)\|\|\|_d)}{\|\|\|\varepsilon(\boldsymbol{\sigma}-\boldsymbol{\sigma}_h)\|\|\|_d}$	11.04	8.38	5.98	4.38	3.18
$\left\|\left\|\left\|u - u_h^R\right\|\right\|\right\|_e$	0.0990	0.0749	0.0524	0.0371	0.0256
$\mathbf{U}(\left\|\left\|\left\|u - u_h^R\right\|\right\|\right\|_e)$	0.994	0.754	0.0532	0.0381	0.0270
$\frac{\mathbf{U}(\left\|\left\|\left\|u-i_h^R\right\|\right\|\right\|_e)}{\left\|\left\|\left\|u-u_h^R\right\|\right\|\right\|_e}$	1.34	1.16	1.09	1.07	1.08

Furthermore, $b \equiv 1$ implies that

$$\mathbf{U}\left(|||\varepsilon(\boldsymbol{\sigma}-\boldsymbol{\sigma}_h)|||_d\right) = \mathbf{U}\left(\left|\left|\left|u-u_h^R\right|\right|\right|_e\right)$$

is the bound provided by Theorem 4.1 and 4.3, which as we see from Table 5 is a fairly sharp upper bound for the errors in our approximations of the flux and primary variables.

Acknowledgements The authors are grateful to the anonymous referee for his/her careful reading and helpful suggestions to improve the presentation of this paper.

Declarations

Conflict of interest The authors have no competing interests to declare that are relevant to the content of this article.

References

1. Ainsworth, M., Babuška, I.: Reliable and robust a posteriori error estimating for singularly perturbed reaction–diffusion problems. SIAM J. Numer. Anal. **36**(2), 331–353 (1999)
2. Ainsworth, M., Vejchodský, T.: Fully computable robust a posteriori error bounds for singularly perturbed reaction–diffusion problems. Numer. Math. **119**(2), 219–243 (2011)
3. Ainsworth, M., Vejchodský, T.: Robust error bounds for finite element approximation of reaction-diffusion problems with non-constant reaction coefficient in arbitrary space dimension. Comput. Methods Appl. Mech. Eng. **281**, 184–199 (2014)
4. Brezzi, F., Fortin, M.: Mixed and Hybrid Finite Element Methods: Springer Series in Computational Mathematics, vol. 15. Springer, New York (1991)
5. Cai, Z., JaEun, K.: A dual finite element method for a singularly perturbed reaction-diffusion problem. SIAM J. Numer. Anal. 58(3), 1654–1673 (2020)
6. Cheddadi, I., Fučík, R., Prieto, M.I., Vohralík, M.: Guaranteed and robust a posteriori error estimates for singularly perturbed reaction–diffusion problems. M2AN Math. Model. Numer. Anal **43**(5), 867–888 (2009)
7. Chen, L.: iFEM: an integrated finite element method package in MATLAB. lyc102.github.io/ifem/ (2009)
8. Ciarlet, P., Do, M.H., Madiot, F.: A posteriori error estimates for mixed finite element discretizations of the neutron diffusion equations. ESAIM Math. Model. Numer. Anal. **57**(1), 1–27 (2023)
9. Creusé, E., Nicaise, S., Kunert, G.: A posteriori error estimation for the Stokes problem: anisotropic and isotropic discretizations. Math. Models Methods Appl. Sci. **14**(9), 1297–1341 (2004)
10. Demlow, A., Kopteva, N.: Maximum-norm a posteriori error estimates for singularly perturbed elliptic reaction–diffusion problems. Numer. Math. **133**(4), 707–742 (2016)
11. Dörfler, W.: A convergent adaptive algorithm for Poisson's equation. SIAM J. Numer. Anal. **33**(3), 1106–1124 (1996)
12. Durán, R.G., Lombardi, A.L.: Finite element approximation of convection diffusion problems using graded meshes. Appl. Numer. Math. **56**(10–11), 1314–1325 (2006)
13. Ekeland, I., Témam, R.: *Convex analysis and variational problems*, volume 28 of *Classics in Applied Mathematics*. Society for Industrial and Applied Mathematics (SIAM), Philadelphia, PA, english edition, (1999). Translated from the French
14. Ern, A., Guermond, J.-L.: Theory and Practice of Finite Elements: Applied Mathematical Sciences, vol. 159. Springer, New York (2004)
15. Kopteva, N.: Maximum norm a posteriori error estimate for a 2D singularly perturbed semilinear reaction–diffusion problem. SIAM J. Numer. Anal. **46**(3), 1602–1618 (2008)
16. Kopteva, N.: Maximum-norm a posteriori error estimates for singularly perturbed reaction–diffusion problems on anisotropic meshes. SIAM J. Numer. Anal. **53**(6), 2519–2544 (2015)

17. Kunert, G.: A posterior H^1 error estimation for a singularly perturbed reaction diffusion problem on anisotropic meshes. IMA J. Numer. Anal. **25**(2), 408–428 (2005)
18. Prager, W., Synge, J.L.: Approximations in elasticity based on the concept of function space. Quart. Appl. Math. **5**, 241–269 (1947)
19. Repin, S., Sauter, S., Smolianski, A.: Two-sided a posteriori error estimates for mixed formulations of elliptic problems. SIAM J. Numer. Anal. **45**(3), 928–945 (2007)
20. Roos, H.-G., Stynes, M.: Some open questions in the numerical analysis of singularly perturbed differential equations. Comput. Methods Appl. Math. **15**(4), 531–550 (2015)
21. Scott, L.R., Zhang, S.: Finite element interpolation of nonsmooth functions satisfying boundary conditions. Math. Comp. **54**(190), 483–493 (1990)
22. Smears, I., Vohralík, M.: Simple and robust equilibrated flux a posteriori estimates for singularly perturbed reaction–diffusion problems. ESAIM Math. Model. Numer. Anal. **54**(6), 1951–1973 (2020)
23. Strang, G., Fix, G.J.: An Analysis of the Finite Element Method. Prentice-Hall Series in Automatic Computation. Prentice-Hall Inc, Englewood Cliffs (1973)
24. Verfürth, R.: Robust a posteriori error estimators for a singularly perturbed reaction–diffusion equation. Numer. Math. **78**(3), 479–493 (1998)
25. Vohralík, M.: Unified primal formulation-based a priori and a posteriori error analysis of mixed finite element methods. Math. Comp. **79**(272), 2001–2032 (2010)
26. Zhang, B., Chen, S., Zhao, J.: A posteriori error estimation based on conservative flux reconstruction for nonconforming finite element approximations to a singularly perturbed reaction–diffusion problem on anisotropic meshes. Appl. Math. Comput. **232**, 1062–1075 (2014)

Publisher's Note Springer Nature remains neutral with regard to jurisdictional claims in published maps and institutional affiliations.

Springer Nature or its licensor (e.g. a society or other partner) holds exclusive rights to this article under a publishing agreement with the author(s) or other rightsholder(s); author self-archiving of the accepted manuscript version of this article is solely governed by the terms of such publishing agreement and applicable law.